ADVANCED FUNCTIONAL MATERIALS
www.afm-journal.de

Anomalously Strong Second-Harmonic Generation in GaAs Nanowires via Crystal-Structure Engineering

*Bin Zhang, Jan E. Stehr, Ping-Ping Chen, Xingjun Wang, Fumitaro Ishikawa, Weimin M. Chen, and Irina A. Buyanova**

GaAs-based semiconductors are highly attractive for diverse nonlinear photonic applications, owing to their non-centrosymmetric crystal structure and huge nonlinear optical coefficients. Nanostructured semiconductors, for example, nanowires (NWs), offer rich possibilities to tailor nonlinear optical properties and further enhance photonic device performance. In this study, it is demonstrated highly efficient second-harmonic generation in subwavelength wurtzite (WZ) GaAs NWs, reaching 2.5×10^{-5} W^{-1}, which is about seven times higher than their zincblende counterpart. This enhancement is shown to be predominantly caused by an axial built-in electric field induced by spontaneous polarization in the WZ lattice via electric field-induced second-order nonlinear susceptibility and can be controlled optically and potentially electrically. The findings, therefore, provide an effective strategy for enhancing and manipulating the nonlinear optical response in subwavelength NWs by utilizing lattice engineering.

1. Introduction

Nonlinear optical processes in semiconductor nanostructures can be utilized in a wide range of classical and quantum applications, including on-chip integrated nano-photonic systems,[1–5] nonlinear optical microscopy,[6–8] and sensing.[9,10] The lowest-order nonlinear optical process is second-harmonic generation (SHG) or frequency doubling, where two incident photons of the same frequency, ω, are converted into a new photon with the frequency, 2ω. It offers an efficient and convenient approach for the realization of next-generation frequency references and combs,[2–4] as well as for infrared-to-visible light conversion that can be used in tunable nanoscale light sources[10,11] and for infrared light visualization.[12]

Due to a large surface-to-volume ratio, utilizing nanostructures, for example, nanowires (NWs), for such applications not only is important for efficient miniaturization but also allows one to tailor and enhance the nonlinear response.[10–30] Considering that a dielectric NW represents a naturally formed cavity, strong localization of the fundamental light and highly directional SHG can be achieved due to Mie resonances caused by interference of the cavity modes,[10] and also by integrating the dielectric NWs into plasmonic structures.[27,31–34] An additional degree of freedom in the engineering of the SHG response is provided by the ability to grow NWs with different lattice structures and, therefore, to explore nonlinearity of crystallographic polytypes that cannot be fabricated in bulk under conventional growth conditions. This makes it possible to tailor a polarimetric response of SHG determined by crystal symmetry.[19] Moreover, symmetry breaking (structural discontinuity) at the NW surface and also electric field discontinuity create additional elements in a nonlinear susceptibility tensor.[35] The contribution of surface nonlinearity can be comparable to or even dominant over the bulk SHG depending on the size/diameter of NWs and, therefore, has a profound effect on the SHG intensity.[23,36] It also allows to change the SHG polarization pattern beyond that dictated by the second-order nonlinear susceptibility tensor, $d^{(2)}$, of the bulk material.[22–24,36–38] Efficient SHG has been experimentally demonstrated in various semiconductor NWs, including GaP,[12,22–24] GaNP,[33] CdS,[25–27] ZnS,[28] ZnO,[29,30] and (Al)GaAs.[10,11,13–19,21,39] The (Al)GaAs material system is especially appealing as nonlinear media, as GaAs exhibits large bulk second-order nonlinear optical susceptibility (d_{36} = 370 pm V^{-1} in ZB[40] and d_{33} = 115 pm V^{-1} in wurtzite [WZ][19,37]), rendering GaAs NWs highly attractive for diverse nonlinear photonic devices.

Though required for its optimization, ascertaining the origin of SHG in thin NWs, including GaAs-based NWs, is not trivial. Here, the difficulties arise from the high sensitivity of nonlinear properties to surfaces, interfaces, and defects that are

Dr. B. Zhang, Dr. J. E. Stehr, Prof. W. M. Chen, Prof. I. A. Buyanova
Department of Physics, Chemistry and Biology
Linköping University
Linköping 581 83, Sweden
E-mail: irina.bouianova@liu.se
Dr. P.-P. Chen, Prof. X. Wang
State Key Laboratory of Infrared Physics
Shanghai Institute of Technical Physics
Chinese Academy of Sciences
Shanghai 200083, China
Prof. F. Ishikawa
Graduate School of Science and Engineering
Ehime University
Matsuyama, Ehime 790-8577, Japan

The ORCID identification number(s) for the author(s) of this article can be found under https://doi.org/10.1002/adfm.202104671.

DOI: 10.1002/adfm.202104671

abundant in NWs. Random twins and stacking faults, which are often present in NWs, also enhance spontaneous polarization in WZ NWs.[41] These built-in electric fields may significantly affect the SHG efficiency.[42,43] Until now, however, impacts of these effects on nonlinear properties of GaAs NWs are still largely unexplored and will be investigated in this work. We demonstrate that the SHG conversion efficiency in thin WZ GaAs NWs is substantially enhanced (by ≈7 times) as compared with that in ZB GaAs NWs of the same diameter, reaching a value of 2.5×10^{-5} W^{-1}. The stronger nonlinear response in WZ is independently confirmed by the performed mapping of the SHG response on a single thin GaAs NW with WZ and ZB segments. We attribute it to a reduced surface symmetry and a strong built-in electric field caused by spontaneous polarization in the WZ lattice. Our findings, therefore, demonstrate a high potential of subwavelength-scale WZ GaAs nanostructures for next-generation nonlinear nanophotonics.

2. Results and Discussion

The investigated GaAs NWs were grown by molecular beam epitaxy (MBE) on Si (111) or GaAs (111)B substrates. More details on the NW growth are described in Experimental Section. Several types of NW structures were examined, including ZB and WZ NWs with diameters (d) of around 80–100 nm. Their crystallographic structures were ascertained by using transmission electron microscopy (TEM). All the investigated structures contain structural defects such as rotational twin planes and stacking faults—see Supporting Information, where typical TEM images of the investigated NWs are shown. The ZB NWs also contain WZ inclusions with a length of 250–350 nm, which corresponds to a WZ volume of 8–12%.

Efficient SHG was detected in all investigated structures. The measurement geometry is schematically illustrated in **Figure 1**a (see also Experimental Section). As an example, Figure 1b,c displays a series of SHG spectra measured at room temperature from representative individual WZ GaAs and ZB GaAs NWs. The measurements were performed under various powers of the fundamental light at $\lambda_\omega = 828$ nm. The SHG signal peaks at 414 nm and its intensity increases quadratically with increasing input power (see the insets in Figure 1b,c), therefore confirming its SHG nature. To evaluate its efficiency in different structures, the measurements were conducted under identical conditions for several NWs of the same type. In the experiments, the polarization of the fundamental light was kept parallel to the NW axis in order to avoid possible variations in the pump power density inside the NWs caused by a dielectric contrast between the NW and its surrounding.[44,45] The SHG conversion efficiency was calculated by $\eta = P_{2\omega}/P_\omega^2$, where $P_{2\omega}$ and P_ω represent the power of the measured SHG and the fundamental light, respectively (see also Supporting Information). Interestingly, on average the SHG conversion efficiency in the WZ GaAs NWs is found to be about three times higher than that of the ZB GaAs NWs, reaching a value of 2.5×10^{-5} W^{-1}. This value is among the highest reported for III-V and II-VI NWs, including hybrid plasmonic structures and nanoresonators[15,31,33,34] (see **Table 1**). This result is somewhat unexpected since WZ GaAs was shown to have lower values of the second-order nonlinear coefficients as compared with ZB. The observed enhancement is found to be robust and can be detected within a wide range of pumping photon wavelengths $\lambda_\omega = 755$–920 nm that are available in our experiments.

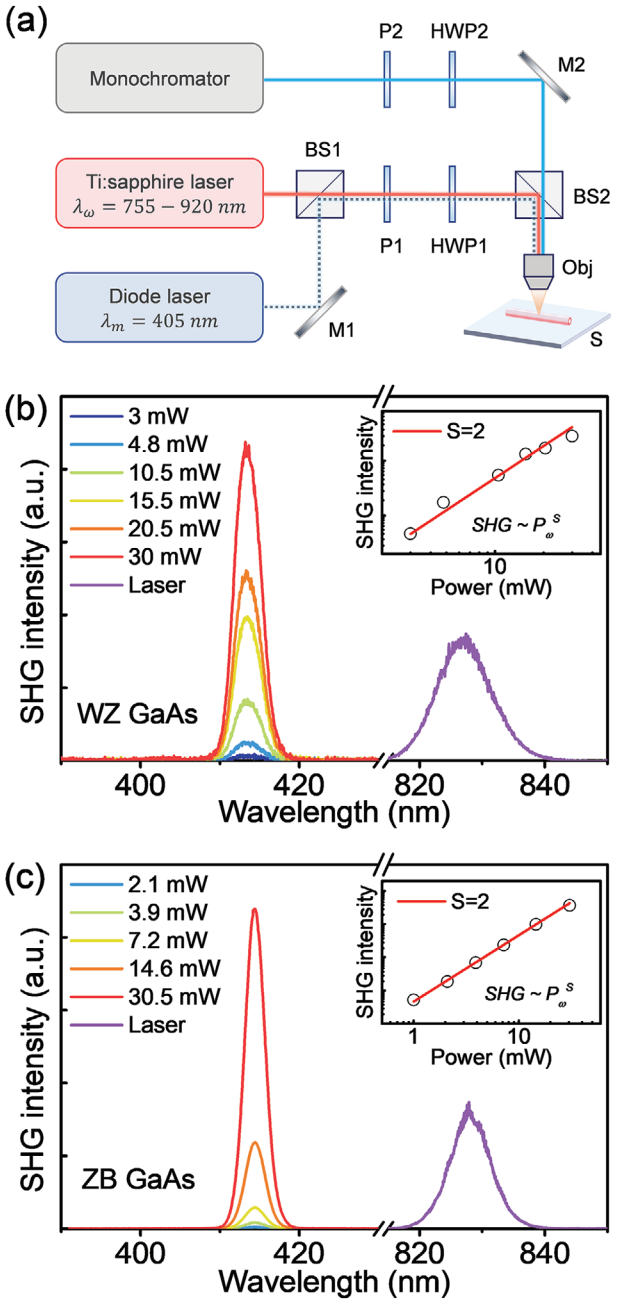

Figure 1. a) A simplified schematic of the set-up for the SHG measurements. The following labels are used: P1, P2—the linear polarizers; HWP1, HWP2—the half-wave plates; BS1, BS2—the beam splitters; M1, M2—the mirrors; Obj—the objective; S—the NW sample transferred onto a silica or gold substrates. A Ti:sapphire laser was used to generate the fundamental light, whereas a 405-nm diode laser was employed in the photomodulation experiments. Representative spectra of the fundamental light and SHG output measured from a single thin b) WZ and thin c) ZB NW at different pumping powers. The insets in (b) and (c) show the integrated SHG intensity (the open circles) as a function of the pumping power P_ω. The solid lines are the best fit to the experimental data by the P_ω^2 function.

Table 1. SHG conversion efficiency measured in this work and reported in the literature. The values determined in this work are averaged among ≈50 NWs.

Sample	SHG conversion efficiency [W^{-1}]	Reference
ZB GaAs NWs	$\approx 1 \times 10^{-5}$	[15]
CdSe NWs	$\approx 4 \times 10^{-5}$	[31]
CdS NWs	$\approx 3 \times 10^{-6}$	[34]
GaNP NWs	$\approx 9.4 \times 10^{-6}$	[33]
ZB GaAs NWs	$\approx 0.78 \times 10^{-5}$	This work
WZ GaAs NWs	$\approx 2.5 \times 10^{-5}$	This work

To further confirm the decisive effect of the crystalline structure on the SHG efficiency, we have performed SHG mapping on individual polytypic GaAs NWs with the crystal structure identified by high-resolution TEM (HRTEM). A representative TEM image of a thin polytypic NW is shown in **Figure 2**b. It can be seen that the NW has an almost straight shape with a diameter of ≈80 nm. The NW crystallized in the WZ crystal phase at the bottom and then transformed to twinned ZB in the middle part and pure ZB phase at the top, as is marked by yellow, green, and blue bars, respectively. Figure 2c–e depicts representative HRTEM images taken from these segments. The transformation of the crystal structure can be clearly distinguished by their fast Fourier transform (FFT) patterns shown in the insets. Knowing the crystalline structures of this NW, we examined its nonlinear response by scanning the tightly focused excitation/detection spot along the NW axis. The so-obtained SHG map, which reflects spatial and spectral distribution of the SHG intensity, is shown in Figure 2a. It is noticeable that the SHG intensity depends on the crystalline structure and increases substantially (by about 6.7 times) in the WZ region. These results therefore provide an unambiguous experimental proof that thin WZ GaAs NWs outperform their ZB counterpart in terms of the nonlinear response.

To understand the dominant mechanism responsible for this effect, we studied polarimetric response of the SHG. For this purpose, the incident electric field $\vec{E}_\omega$ was rotated in the plane, the y–z plane in **Figure 3**a,d, which is orthogonal to the propagation direction of the incident fundamental light and the backscattered SHG light, that is, the x-axis. The intensities of the SHG components linearly polarized parallelly and orthogonally to the NW axis (chosen as the z-axis), denoted below as the parallel (//) and orthogonal (⊥) SHG components, were then measured as a function of the angle θ between $\vec{E}_\omega$ and the NW axis as indicated in Figure 3a,d. Representative polar plots of the measured SHG output from a thin ZB NW are shown by the symbols in Figure 3b,c, which contain two lobes that are oriented along the NW axis. Even though the observed pattern of the dominant parallel SHG component can be explained solely based on the bulk second-order nonlinear susceptibility $d^{(2)}$ (shown by the green solid line in Figure 3b), this is not the case for the orthogonal component (Figure 3c). Since ZB GaAs is a non-centrosymmetric crystal belonging to the $\bar{4}3m$ crystal symmetry group, it has three nonvanishing elements of $d^{(2)ZB}$: $d_{14} = d_{25} = d_{36} = 370$ pm V^{-1}. Therefore, two pairs of two lobes are expected for the ⊥-component generated from a perfect bulk crystal. Their intensity and orientation are determined by the in-coupling and out-coupling coefficients of the fundamental and SHG light, which is defined in thin NWs as $\gamma_{\omega,\,\mathrm{in}} = 2/(1+\varepsilon_\omega)$ and $\gamma_{2\omega,\mathrm{out}} = 2/(1+\varepsilon_{2\omega})$, respectively (see Supporting Information). Here, $\varepsilon_\omega(\varepsilon_{2\omega})$ represents the dielectric constant of the NW at a light frequency of $\omega(2\omega)$. The presence of twin domains corresponding to a 60° rotation of the ZB lattice changes the relative intensity between these two

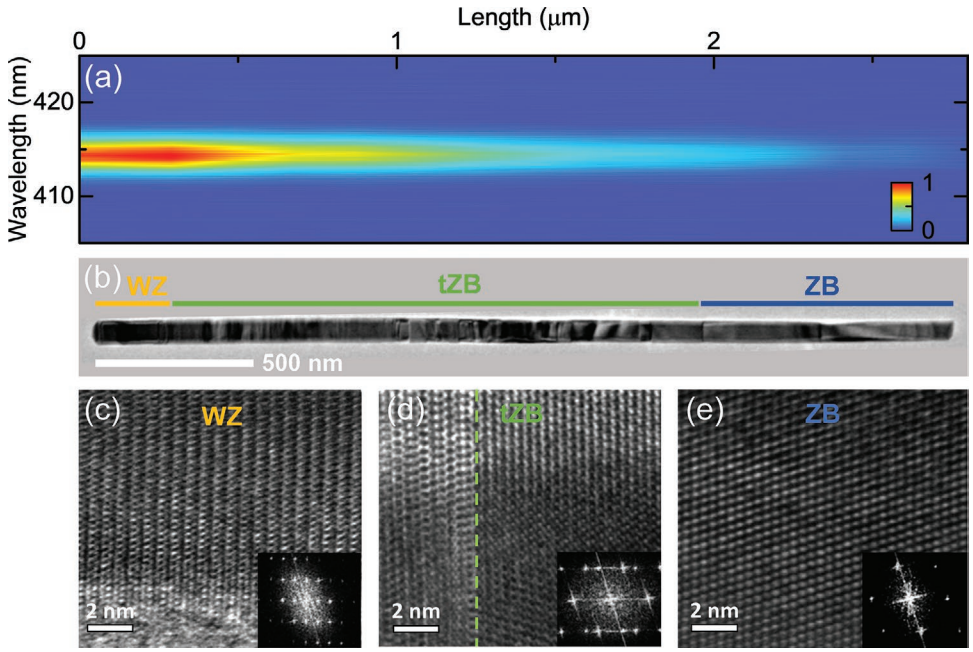

Figure 2. a) Spatial and spectral distribution of the SHG intensity measured along the single polytypic GaAs NW as shown in (b). b) TEM micrograph of the studied GaAs NW. Yellow, green, and blue bars mark the NW regions with predominantly WZ, twinned ZB (tZB), and ZB crystal structure, respectively. High-resolution TEM images with the corresponding FFT patterns obtained from c) WZ, d) tZB, and e) ZB regions, respectively. The dashed green line in (d) indicates location of the twinned plane.

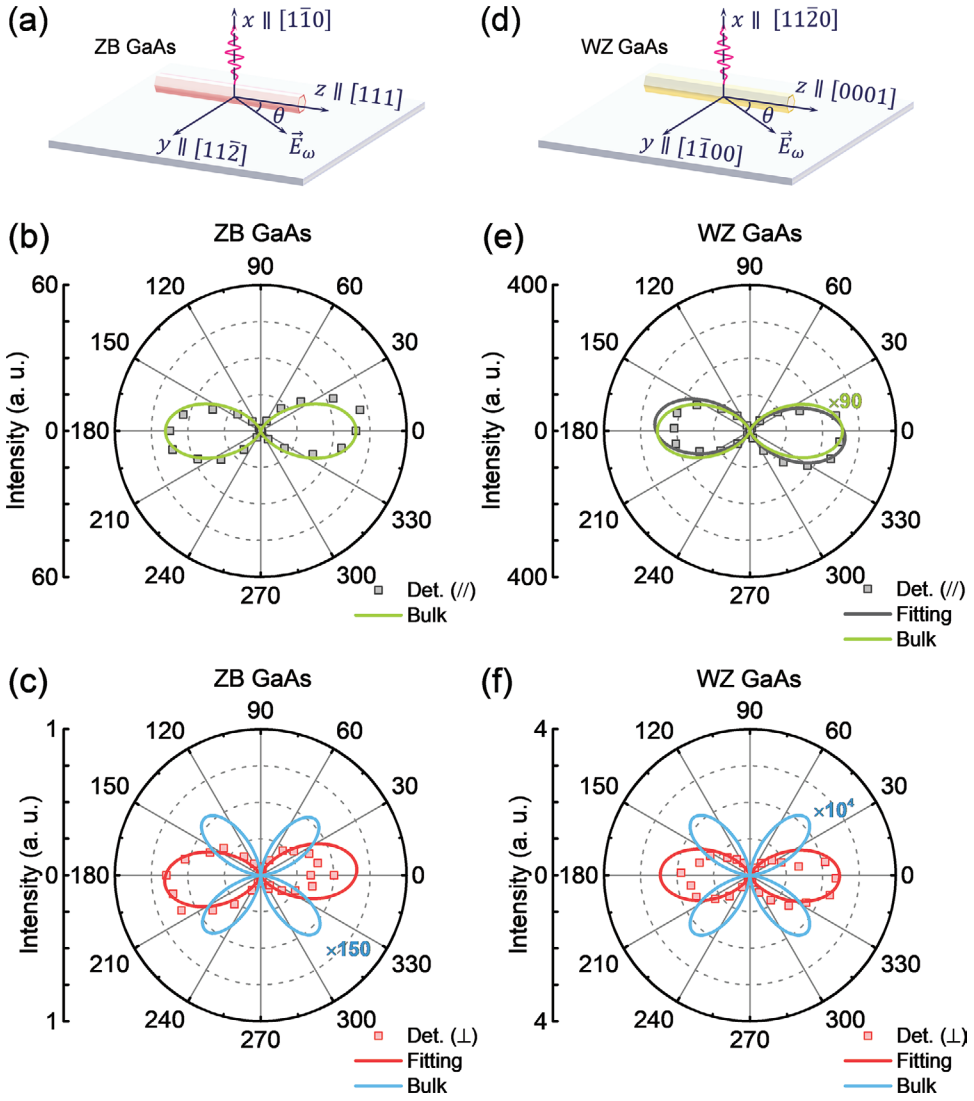

Figure 3. The measurement geometry utilized in the polarization-resolved SHG experiments on individual a) ZB and d) WZ NWs. $\vec{E}_\omega$ is the direction of the fundamental electric field that was rotated in the substrate plane by an angle θ relative to the NW axis (chosen as the *z*-direction). Polar plots of the b,e) parallel and c,f) orthogonal SHG output measured from a thin ZB (b,c) and thin WZ (e,f) GaAs NWs. The symbols represent experimental data. The green and blue solid lines are the expected SHG responses based on the bulk nonlinear susceptibility for the//- and ⊥-components, respectively. The black and red lines show the modeled SHG responses by taking into account the surface effect and electric-field induced SHG.

pairs as determined by the weighted contribution of both dom ains.[13,14,16,19,46] The expected polar pattern is shown by the blue line in Figure 3c assuming that the two domains are present with the weight ratio of 0.53:0.47, as revealed by TEM. Such polarimetric pattern is indeed detected from our reference thick ZB NWs with $d \approx 400$ nm (see Supporting Information). On the other hand, it obviously disagrees with the experimental data from the thin ZB NWs shown in Figure 3c in terms of the polar pattern and intensity of the ⊥-polarized SHG component. The latter exhibits only one pair of lobes, but with a much stronger intensity.

Even stronger deviations of the measured polar plots from the expected polarimetric pattern in bulk are observed in thin WZ NWs. The corresponding results are shown by the symbols in Figure 3e,f for the //- and ⊥-component, respectively. Indeed, in the case of bulk WZ GaAs that belongs to the *6mm* point group,[19,37] the second-order nonlinear susceptibility tensor, $d^{(2)WZ}$, has three independent components: $d_{33} = 115$ pm V^{-1}, $d_{15} = d_{24} = 53$ pm V^{-1}, $d_{31} = d_{32} = 26$ pm V^{-1}.[37] Since the intensity of the //-component is determined by d_{33}, one would expect a significant decrease of the //-component in WZ as compared with ZB, by about 13.8 times (shown by the green solid line in Figure 3e). This is in a stark contrast with the opposite trend found from our experimental data, which shows an intensity increase by about 6.7 times (shown by the symbols in Figure 3e). In addition, a polarimetric pattern with four lobes of an equal magnitude is expected for the ⊥-component in bulk WZ GaAs. Such SHG response is drastically different from our experimental data featuring a two-lobe pattern (see Figure 3f). Moreover, a significantly higher intensity of this component is also observed as compared with the expected bulk contribution.

The observed drastic increase in the intensity of the orthogonal SHG component and the change of its polar pattern in thin WZ and ZB NWs can be explained by considering a surface contribution to the SHG response, induced by the reduced crystal symmetry at the NW surface. This contribution is expected to become pronounced for thin NWs because of an increased surface-to-volume ratio. Within the commonly used cylindric approximation,[36,38] breaking of the inversion symmetry at the NW surface leads to three new nonvanishing components (d^S_{yyy}, d^S_{yzz}, and d^S_{zzy}) of the second-order nonlinear susceptibility tensor. By including these surface components, the excitation-polarization response of the ⊥-component is transformed into nearly perfect two-lobe pattern (see Supporting Information). The experimental data can be modeled by including surface nonlinear terms $d^S : d^{S,ZB}_{yzz} = 1.076 d_{36}, d^{S,ZB}_{zzy} = 0.723 d_{36}$; and $d^{S,WZ}_{yzz} = 2.094 d_{36}, d^{S,WZ}_{zzy} = 1.841 d_{36}$—see the red curves in Figure 3c,f. (Here, all values are given relative to the d_{36} value of ZB, for easy comparison). We note that the deduced values are higher in WZ NWs. This could be tentatively attributed to lower symmetry of the WZ surface as compared with ZB, which is not taken into account within the used cylindric approximation.

The surface contribution enhances the SHG radiation that is polarized normal to the surface of thin NWs. However, its influence on the dominant SHG output parallel to the NW axis is expected to be negligible.[36] It thus cannot account for the dramatic increase of this SHG component that occurs in our thin WZ NWs (see Figure 3e). To model this enhancement of the SHG response (shown by the black line in Figure 3e) we need to assume $d^{eff}_{zzz} = 9.6 d_{33}$. We explain this by considering that WZ semiconductors experience spontaneous polarization and an internal electric field along the crystallographic *c*-axis due to distortion of $GaAs_4$ tetrahedron in WZ.[41] Such field was shown to be substantial in WZ NWs due to the presence of structural defects, such as twins and stacking faults.[41,47,48] A static electric field E^{DC}_l may lead to an enhancement of the second-order nonlinear process due to its interaction with the third-order nonlinear coefficients $d^{(3)}_{ijkl}$, which results in an effective second-order nonlinear susceptibility $d^{eff}_{ijk} = d^{(2)}_{ijk} + d^{(3)}_{ijkl} E^{dc}_l$.[25,42,49] Here, *i*, *j*, *k*, *l* are the Cartesian indices and the index *l* defines the direction of the electric field. This often causes a dramatic enhancement of the SHG efficiency, which can be controlled by E^{DC}_l.[25,49,50] Since the built-in field due to spontaneous polarization is directed along the NW axis, that is, $l = z$, the electric-field induced SHG (EFISH) defined by $d^{(3)}_{zzzz} E^{DC}_z$ may enhance the parallel SHG component in WZ NWs and, therefore, their overall nonlinear output (see also Supporting Information).

To verify the proposed mechanism, we performed polarization-resolved photo-modulation SHG measurements. In these experiments, an additional laser with photon energy higher than the GaAs bandgap was used to create free carriers and modulate the built-in electric field[42,43,51] (see Figure 1a). Both the modulation (λ_m = 405 nm) and pump (λ_ω = 920 nm) light were set to be linearly polarized in the direction parallel to the NW axis to ensure maximum in-coupling. If the built-in electric field indeed plays a constructive role in the SHG response, partial screening of this field caused by the presence of free carriers is expected to suppress the EFISH-induced output. This is indeed observed experimentally. As can be seen from the **Figure 4**a,b, the parallel SHG component in thin WZ NWs is reduced by about 27% when the 405-nm light illumination is switched on, whereas the variation of the perpendicular component under these conditions remains below the detection limit. On the other hand, only a minor decrease of the parallel SHG output is detected in thin ZB NWs (see the lower panel in Figure 4b). These results provide an unambiguous experimental proof that the built-in field due to spontaneous polarization of the WZ lattice dramatically enhances the nonlinear response of GaAs NWs. They also show that this response can be efficiently controlled by changing the strength of the built-in electric field either optically or electrically.

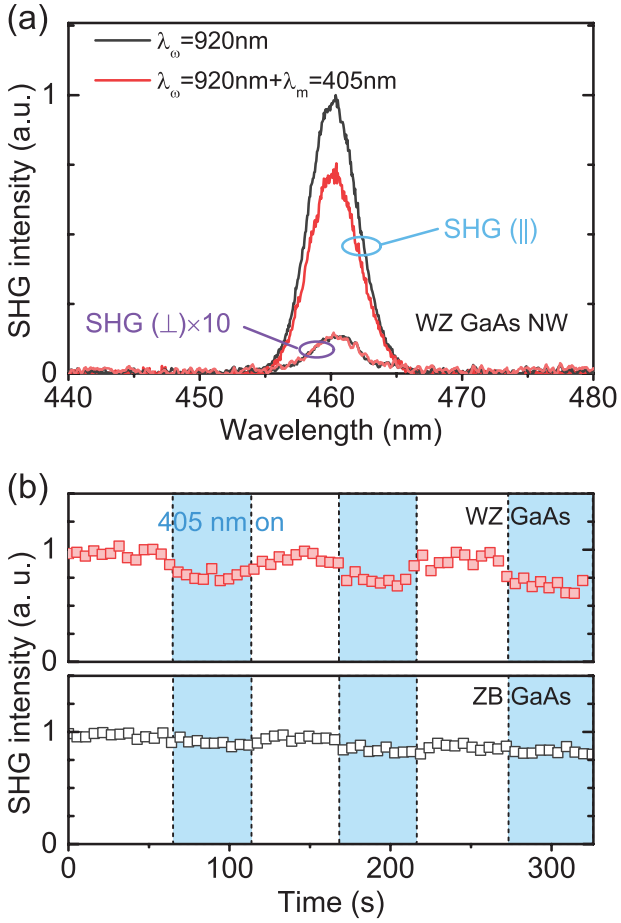

Figure 4. a) The SHG spectra of a single thin WZ GaAs NW with (the red curves) and without (the black curves) the additional 405-nm light illumination. The labels //and ⊥ define the polarization of the measured SHG output. b) Time evolution of the //SHG output from thin WZ (the red filled squares) and thin ZB (the black open squares) GaAs NWs under photo-modulation with the 405-nm light. The blue shaded areas show the SHG response with the modulation light on.

3. Conclusion

In summary, we have investigated nonlinear optical properties of thin GaAs NWs with ZB and WZ crystal structures. The SHG intensity was found to be significantly stronger in WZ NWs as compared with ZB NWs (by about seven times), reaching the value of 2.5×10^{-5} W^{-1}. This value is among the

highest reported in the literature, including complex waveguide and nanoresonator structures, as well as hybrid plasmonic structures.[15,31,33,34] Such enhancement was directly verified by correlative SHG intensity mapping and TEM characterization performed on the same polymorphic NWs. Polarization-resolved measurements shows that the increase of the orthogonal SHG component is chiefly controlled by the surface-induced SHG caused by structural and electric field discontinuity at the NW surface. This component, however, remains weaker than the parallel SHG output, by about two orders of magnitude, due to weak out-coupling of the generated light from thin NWs. The dominant parallel SHG is proven to be enhanced in WZ via EFISH, which is activated by the axial built-in electric field related to spontaneous polarization in WZ NWs, and can be controlled optically and potentially electrically. This SHG enhancement is found to be robust and does not require high structural quality of the NWs as the presence of structural defects in fact facilitates SHG by enhancing the internal electric field.[41] A more precise control of crystalline structure in MBE-grown NWs could be achievable in future by fine tuning As and Ga fluxes during the growth.[52] Our results, therefore, demonstrate great potential of thin GaAs NWs for nonlinear nanophotonics and show that their nonlinear properties can be manipulated via lattice engineering.

4. Experimental Section

The WZ GaAs NWs investigated in this work were grown by MBE on GaAs (111)B substrates using Au as a catalyst. During the growth process, the substrate temperature was kept at ≈353 °C, and the As_4/Ga beam equivalent pressure (BEP) ratio was set to ≈30.[44,53] Thin ZB GaAs NWs were synthesized by constituent Ga-catalyzed MBE on Si (111) substrates. To obtain regularly structured NWs with a high vertical yield, prior to the growth, the n-type Si(111) substrate surface was heated to 760 °C and surface native oxide was removed by Ga irradiation. After the treatment, the substrate temperature was reduced to 630 °C. As_4 BEP was set to 4×10^{-6} Torr and the Ga flux was set to match a planar growth rate of 1.0 ML s^{-1} on GaAs (001). The Ga flux was supplied on the substrate surface for 45 s. Then NWs growth was initiated by supplying As flux and the NWs were grown by keeping the Ga and As flux for 15 min. Reference thick NWs (with a diameter around 400 nm) were fabricated by continuing the radial growth for 30 min. Crystalline structure of the NWs was analyzed utilizing TEM performed using a FEI Tecnai G2 TF20 UT system. Samples for TEM investigations were prepared by mechanical transfer of NWs onto a carbon/copper TEM grid.

Nonlinear optical measurements were performed on individual lying NWs that were transferred onto gold or silica substrates and positioned on an *x*–*y* stage. The measurements were conducted using a confocal Horiba Jobin Yvon HR800 system equipped with a cooled charge coupled device. Schematic of the measurement set-up is shown in Figure 1a. A wavelength-tunable mode-locked Ti:sapphire laser with a repetition frequency of ≈76 MHz and a pulse duration of ≈150 fs was employed as the fundamental light source with $\lambda_\omega = 755$–920 nm. Its polarization was controlled by a linear polarizer (P1) and a half-wave plate (HWP1) (see Figure 1a). The estimated diameter of the laser spot was ≈1.9 µm, which was dictated by the diffraction limit, and the effective detection area of the SHG light was ≈0.6 µm in diameter. The induced SHG signal was collected by a long focal length objective (50×, NA = 0.5) in a strict backscattering geometry. The desired polarization of the SHG light was selected by using a rotatable half-wave plate (HWP2) together with a fixed linear polarizer (P2). In photo-modulation SHG measurements, a 405 nm diode laser was used for modulation of the SHG signal, in addition to the fundamental light source. Its power was kept below 1 mW μm^{-2} to avoid heating effects.

Supporting Information

Supporting Information is available from the Wiley Online Library or from the author.

Acknowledgements

The authors would like to acknowledge the financial support from the Swedish Research Council (Grant No. 2019-04312) and the Swedish Foundation for International Cooperation in Research and Higher Education (STINT) (Grant No. JA2014-5698). I.A.B. and W.M.C. acknowledge financial support from the Swedish Government Strategic Research Area in Materials Science on Functional Materials at Linköping University (Faculty Grant SFO-Mat-LiU No 2009 00971). The NW growth was supported by KAKENHI (Grants Nos. 19H00855 and 16H05970) from Japan Society of Promotion of Science and National Natural Science Foundation of China (12027805 and 11991060).

Conflict of Interest

The authors declare no conflict of interest.

Data Availability Statement

Research data are not shared.

Keywords

GaAs, nanowires, second harmonic generation, spontaneous polarization, wurtzite

Received: May 17, 2021
Revised: June 8, 2021
Published online: June 24, 2021

[1] R. Kirchain, L. Kimerling, *Nat. Photonics* **2007**, *1*, 303.
[2] X. Y. Lu, G. Moille, A. Rao, D. A. Westly, K. Srinivasan, *Nat. Photonics* **2021**, *15*, 131.
[3] X. Xue, F. Leo, Y. Xuan, J. A. Jaramillo-Villegas, P. H. Wang, D. E. Leaird, M. Erkintalo, M. Qi, A. M. Weiner, *Light: Sci. Appl.* **2017**, *6*, e16253.
[4] L. Chang, A. Boes, P. Pintus, J. D. Peters, M. J. Kennedy, X. W. Guo, N. Volet, S. P. Yu, S. B. Papp, J. E. Bowers, *APL Photonics* **2019**, *4*, 036103.
[5] Y. Huang, X. Duan, C. M. Lieber, *Small* **2005**, *1*, 142.
[6] Y. Nakayama, P. J. Pauzauskie, A. Radenovic, R. M. Onorato, R. J. Saykally, J. Liphardt, P. Yang, *Nature* **2007**, *447*, 1098.
[7] P. Pantazis, J. Maloney, D. Wu, S. E. Fraser, *Proc. Natl. Acad. Sci. USA* **2010**, *107*, 14535.
[8] H. Harutyunyan, S. Palomba, J. Renger, R. Quidant, L. Novotny, *Nano Lett.* **2010**, *10*, 5076.
[9] S. Kim, K. H. Kim, D. J. Hill, H. G. Park, J. F. Cahoon, *Nat. Commun.* **2018**, *9*, 2781.
[10] L. Xu, G. Saerens, M. Timofeeva, D. A. Smirnova, I. Volkovskaya, M. Lysevych, R. Camacho-Morales, M. Cai, K. Z. Kamali, L. J. Huang, F. Karouta, H. H. Tan, C. Jagadish, A. E. Miroshnichenko, R. Grange, D. N. Neshev, M. Rahmani, *ACS Nano* **2020**, *14*, 1379.
[11] G. Saerens, I. Tang, M. I. Petrov, K. Frizyuk, C. Renaut, F. Timpu, M. R. Escale, I. Shtrom, A. Bouravleuv, G. Cirlin, R. Grange, M. Timofeeva, *Laser Photonics Rev.* **2020**, *14*, 2000028.

[12] V. V. Fedorov, A. Bolshakov, O. Sergaeva, V. Neplokh, D. Markina, S. Bruyere, G. Saerens, M. I. Petrov, R. Grange, M. Timofeeva, S. V. Makarov, I. S. Mukhin, *ACS Nano* **2020**, *14*, 10624.
[13] H. He, X. Q. Zhang, X. Yan, L. L. Huang, C. L. Gu, M. L. Hu, X. Zhang, X. M. Ren, C. Y. Wang, *Appl. Phys. Lett.* **2013**, *103*, 143110.
[14] R. Grange, G. Bronstrup, M. Kiometzis, A. Sergeyev, J. Richter, C. Leiterer, W. Fritzsche, C. Gutsche, A. Lysov, W. Prost, F. J. Tegude, T. Pertsch, A. Tunnermann, S. Christiansen, *Nano Lett.* **2012**, *12*, 5412.
[15] J. Wang, Y. Yu, Y. M. Wei, S. F. Liu, J. Li, Z. K. Zhou, Z. C. Niu, S. Y. Yu, X. H. Wang, *Sci. Rep.* **2017**, *7*, 2166.
[16] A. C. S. Pimenta, D. C. T. Ferreira, D. B. Roa, M. V. B. Moreira, A. G. de Oliveira, J. C. Gonzalez, M. De Giorgi, D. Sanvitto, F. M. Matinaga, *J. Phys. Chem. C* **2016**, *120*, 17046.
[17] L. Carletti, D. de Ceglia, M. A. Vincenti, C. De Angelis, *Opt. Express* **2019**, *27*, 32480.
[18] S. Liu, M. B. Sinclair, S. Saravi, G. A. Keeler, Y. Yang, J. Reno, G. M. Peake, F. Setzpfandt, I. Staude, T. Pertsch, I. Brener, *Nano Lett.* **2016**, *16*, 5426.
[19] M. Timofeeva, A. Bouravleuv, G. Cirlin, I. Shtrom, I. Soshnikov, M. Reig Escale, A. Sergeyev, R. Grange, *Nano Lett.* **2016**, *16*, 6290.
[20] M. Timofeeva, L. Lang, F. Timpu, C. Renaut, A. Bouravleuv, I. Shtrom, G. Cirlin, R. Grange, *Nano Lett.* **2018**, *18*, 3695.
[21] J. D. Sautter, L. Xu, A. E. Miroshnichenko, M. Lyseyych, I. Volkoyskaya, D. A. Smirnova, R. Camacho-Morales, K. Z. Kamali, F. Karouta, K. Vora, H. H. Tan, M. Kauranen, I. Staude, C. Jagadish, D. N. Neshev, M. Rahmani, *Nano Lett.* **2019**, *19*, 3905.
[22] R. Sanatinia, S. Anand, M. Swillo, *Nano Lett.* **2014**, *14*, 5376.
[23] R. Sanatinia, M. Swillo, S. Anand, *Nano Lett.* **2012**, *12*, 820.
[24] R. Sanatinia, S. Anand, M. Swillo, *Opt. Express* **2015**, *23*, 756.
[25] M. L. Ren, J. S. Berger, W. Liu, G. Liu, R. Agarwal, *Nat. Commun.* **2018**, *9*, 186.
[26] M. L. Ren, R. Agarwal, W. Liu, R. Agarwal, *Nano Lett.* **2015**, *15*, 7341.
[27] X. F. Liu, Q. Zhang, W. K. Chong, J. N. Yip, X. L. Wen, Z. P. Li, F. X. Wei, G. N. Yu, Q. H. Xiong, T. C. Sum, *ACS Nano* **2015**, *9*, 5018.
[28] H. Hu, K. Wang, H. Long, W. Liu, B. Wang, P. Lu, *Nano Lett.* **2015**, *15*, 3351.
[29] M. C. Larciprete, M. Centini, *Appl. Phys. Rev.* **2015**, *2*, 031302.
[30] X. B. Han, K. Wang, H. Long, H. B. Hu, J. W. Chen, B. Wang, P. X. Lu, *ACS Photonics* **2016**, *3*, 1308.
[31] J. Shi, Y. Li, M. Kang, X. He, N. J. Halas, P. Nordlander, S. Zhang, H. Xu, *Nano Lett.* **2019**, *19*, 3838.
[32] G. Grinblat, M. Rahmani, E. Cortes, M. Caldarola, D. Comedi, S. A. Maier, A. V. Bragas, *Nano Lett.* **2014**, *14*, 6660.
[33] Z. Luo, C. Ma, Y. Lin, Q. Jiang, B. Liu, X. Yang, X. Yi, J. Qu, X. Zhu, X. Wang, J. Zhou, X. Wang, W. M. Chen, I. A. Buyanova, S. Chen, A. Pan, *Nano Lett.* **2021**, *21*, 3426.
[34] M. L. Ren, W. Liu, C. O. Aspetti, L. Sun, R. Agarwal, *Nat. Commun.* **2014**, *5*, 5432.
[35] P. Guyot-Sionnest, W. Chen, Y. R. Shen, *Phys. Rev. B* **1986**, *33*, 8254.
[36] Y. M. Wei, Y. Yu, J. Wang, L. Liu, H. Q. Ni, Z. C. Niu, J. T. Li, X. H. Wang, S. Y. Yu, *Nanoscale* **2017**, *9*, 16066.
[37] R. Chen, S. Crankshaw, T. Tran, L. C. Chuang, M. Moewe, C. Chang-Hasnain, *Appl. Phys. Lett.* **2010**, *96*, 051110.
[38] P. R. Wiecha, A. Arbouet, C. Girard, T. Baron, V. Paillard, *Phys. Rev. B* **2016**, *93*, 125421.
[39] M. Timofeeva, L. Lang, F. Timpu, C. Renaut, A. Bouravleuv, I. Shtrom, G. Cirlin, R. Grange, *Nano Lett.* **2018**, *18*, 3695.
[40] R. W. Boyd, *Nonlinear Optics*, Academic Press, Cambridge, MA **2008**.
[41] B. Bauer, J. Hubmann, M. Lohr, E. Reiger, D. Bougeard, J. Zweck, *Appl. Phys. Lett.* **2014**, *104*, 211902.
[42] T. A. Germer, K. W. Kolasinski, J. C. Stephenson, L. J. Richter, *Phys. Rev. B* **1997**, *55*, 10694.
[43] Y. M. Chang, Y. L. Hong, S. Gwo, *Appl. Phys. Lett.* **2008**, *93*, 131106.
[44] B. Zhang, Y. Huang, J. E. Stehr, P. P. Chen, X. J. Wang, W. Lu, W. M. Chen, I. A. Buyanova, *Nano Lett.* **2019**, *19*, 6454.
[45] H. E. Ruda, A. Shik, *Phys. Rev. B* **2005**, *72*, 115308.
[46] M. L. Ren, R. Agarwal, P. Nukala, W. Liu, R. Agarwal, *Nano Lett.* **2016**, *16*, 4404.
[47] L. Li, L. Jin, J. Wang, D. J. Smith, W. J. Yin, Y. Yan, H. Sang, W. C. Choy, M. R. McCartney, *Adv. Mater.* **2012**, *24*, 1328.
[48] L. Y. Li, Z. F. Gan, M. R. McCartney, H. S. Liang, H. B. Yu, W. J. Yin, Y. F. Yan, Y. H. Gao, J. B. Wang, D. J. Smith, *Adv. Mater.* **2014**, *26*, 1052.
[49] D. Brunne, M. Lafrentz, V. V. Pavlov, R. V. Pisarev, A. V. Rodina, D. R. Yakovlev, M. Bayer, *Phys. Rev. B* **2015**, *92*, 085202.
[50] E. Timurdogan, C. V. Poulton, M. J. Byrd, M. R. Watts, *Nat. Photonics* **2017**, *11*, 200.
[51] J. Qi, M. Yeganeh, I. Koltover, A. Yodh, W. Theis, *Phys. Rev. Lett.* **1993**, *71*, 633.
[52] F. Panciera, Z. Baraissov, G. Patriarche, V. G. Dubrovskii, F. Glas, L. Travers, U. Mirsaidov, J.-C. Harmand, *Nano Lett.* **2020**, *20*, 1669.
[53] Z. Lu, Z. Zhang, P. Chen, S. Shi, L. Yao, C. Zhou, X. Zhou, J. Zou, W. Lu, *Appl. Phys. Lett.* **2014**, *105*, 162102.